Dynamics of femtosecond supercontinuum generation in multimode fibers

Francesco Poletti and Peter Horak
Optoelectronics Research Centre, University of Southampton, SO17 1BJ, United Kingdom
frap@orc.soton.ac.uk, peh@orc.soton.ac.uk

Abstract: We solve a system of generalized nonlinear Schrödinger equations to study the nonlinear dynamics of ultrashort pulse propagation in multimode fibers. Due to pulse walk-off, permanent intermodal power transfer between modes is observed even in absence of phase matching. The strength of intermodal effects is found to depend strongly on modal symmetries, which results in preferential coupling between the LP_{0n} modes. The scaling of nonlinear multimode effects in large-core fibers for the generation of ultra-high power spectral density supercontinua is finally discussed.

OCIS codes: (190.4370) Nonlinear optics, fibers; (190.5530) Pulse propagation and temporal solitons; (190.7110) Ultrafast nonlinear optics; (320.6629) Supercontinuum generation.

References and links

1. R. R. Alfano and S. L. Shapiro, "Observation of self-phase modulation and small-scale filaments in crystals and glasses," Phys. Rev. Lett. **24**, 592–594 (1970).
2. G. Genty, S. Coen, and J. M. Dudley, "Fiber supercontinuum sources (Invited)," J. Opt. Soc. Am. B **24**, 1771-1785 (2007), http://www.opticsinfobase.org/josab/abstract.cfm?URI=josab-24-8-1771.
3. J. H. V. Price, T. M. Monro, H. Ebendorff-Heidepriem, F. Poletti, P. Horak, V. Finazzi, J. Y. Y. Leong, P. Petropoulos, J. C. Flanagan, G. Brambilla, X. Feng and D. J. Richardson, "Mid-IR supercontinuum generation from non-silica microstructured fibers," IEEE J. Sel. Top. Quantum Electron. **13**, 738–749 (2007).
4. A. Kudlinski, A. K. George, J. C. Knight, J. C. Travers, A. B. Rulkov, S. V. Popov, and J. R. Taylor, "Zero-dispersion wavelength decreasing photonic crystal fibers for ultraviolet-extended supercontinuum generation," Opt. Express 14, 5715-5722 (2006), http://www.opticsinfobase.org/abstract.cfm?URI=oe-14-12-5715.
5. J. M. Dudley, G. Genty, and S. Coen, "Supercontinuum generation in photonic crystal fiber," Rev. Mod. Phys. **78**, 1135–1184 (2006).
6. T. Brabec and F. Krausz, "Nonlinear optical pulse propagation in the single-cycle regime," Phys. Rev. Lett. **78**, 3282–3285 (1997).
7. M. Kolesik and J. V. Moloney, "Nonlinear optical pulse propagation: From Maxwell's to unidirectional equations," Phys. Rev. E **70**, 036604 (2004).
8. B. A. Cumberland, J. C. Travers, S. V. Popov, and J. R. Taylor, "29 W High power CW supercontinuum source," Opt. Express **16**, 5954–5962 (2008), http://www.opticsinfobase.org/abstract.cfm?URI=oe-16-8-5954.
9. A. Efimov, A. J. Taylor, F. G. Omenetto, J. C. Knight, W. J. Wadsworth, and P. St. J. Russell, "Nonlinear generation of very high-order UV modes in microstructured fibers," Opt. Express **11**, 910–918 (2003).
10. J. H. V. Price, T. M. Monro, K. Furusawa, W. Belardi, J. C. Baggett, S. Coyle, C. Netti, J. J. Baumberg, R. Paschotta, and D. J. Richardson, "UV generation in a pure-silica holey fiber," Appl. Phys. B **77**, 291–298 (2003).
11. T. Delmonte, M. A. Watson, E. J. O'Driscoll, X. Feng, T. M. Monro, V. Finazzi, P. Petropoulos, J. H. V. Price, J. C. Baggett, W. Loh, D. J. Richardson, and D. P. Hand, "Generation of mid-IR continuum using tellurite microstructured fiber," in Conference on Lasers and Electro-Optics, paper CTuA4, Long Beach, USA (2006).
12. V. L. Kalashnikov, E. Sorokin, and I. T. Sorokina, "Spatial-temporal structure of the femtosecond third harmonic generation in photonic-crystal fibers," Opt. Express **15**, 11301-11312 (2007), http://www.opticsinfobase.org/abstract.cfm?URI=oe-15-18-11301.
13. G. P. Agrawal, *Nonlinear Fiber Optics*, 3rd ed. (Academic Press, San Diego, CA, USA, 2001).

#106238 - $15.00 USD Received 12 Jan 2009; revised 11 Feb 2009; accepted 16 Feb 2009; published 1 Apr 2009

14. S. Coen, A. H. L. Chau, R. Leonhardt, J. D. Harvey, J. C. Knight, W. J. Wadsworth, and P. St. J. Russell, "Supercontinuum generation by stimulated Raman scattering and parametric four-wave mixing in photonic crystal fibers," J. Opt. Soc. Am. B **19**, 753–764 (2002).
15. M. Lehtonen, G. Genty, H. Ludvigsen, and M. Kaivola, "Supercontinuum generation in a highly birefringent microstructured fiber," Appl. Phys. Lett. **82**, 2197–2199 (2003).
16. E. R. Martins, D. H. Spadoti, M. A. Romero, and B.-H. V. Borges, "Theoretical analysis of supercontinuum generation in a highly birefringent D-shaped microstructured optical fiber," Opt. Express **15**, 14335-14347 (2007).
17. J. M. Dudley, L. Provino, N. Grossard, H. Maillotte, R. S. Windeler, B. J. Eggleton, and S. Coen, "Supercontinuum generation in air-silica microstructured fibers with nanosecond and femtosecond pulse pumping," J. Opt. Soc. Am. B **19**, 765–771 (2002).
18. A. Tonello, S. Pitois, S. Wabnitz, G. Millot, T. Martynkien, W. Urbanczyk, J. Wojcik, A. Locatelli, M. Conforti, and C. De Angelis, "Frequency tunable polarization and intermodal modulation instability in high birefringence holey fiber," Opt. Express **14**, 397–404 (2006) http://www.opticsinfobase.org/oe/abstract.cfm?URI=oe-14-1-397.
19. C. Lesvigne, V. Couderc, A. Tonello, P. Leproux, A. Barthelemy, S. Lacroix, F. Druon, P. Blandin, M. Hanna, and P. Georges, "Visible supercontinuum generation controlled by intermodal four-wave mixing in microstructured fiber," Opt. Lett. **32**, 2173-2175 (2007), http://www.opticsinfobase.org/ol/abstract.cfm?URI=ol-32-15-2173.
20. F. Poletti and P. Horak, "Description of ultrashort pulse propagation in multimode optical fibers," J. Opt. Soc. Am. B **25**, 1645–1654 (2008) http://www.opticsinfobase.org/josab/abstract.cfm?URI=josab-25-10-1645.
21. R. Cherif, M. Zghal, L. Tartara, and V. Degiorgio, "Supercontinuum generation by higher-order mode excitation in a photonic crystal fiber," Opt. Express **16**, 2147–2152 (2008) http://www.opticsinfobase.org/oe/abstract.cfm?URI=oe-16-3-2147.
22. F. Poletti, V. Finazzi, T. M. Monro, N. G. R. Broderick, V. Tse, and D. J. Richardson, "Inverse design and fabrication tolerances of ultra-flattened dispersion holey fibers," Opt. Express **13**, 3728-3736 (2005), http://www.opticsinfobase.org/oe/abstract.cfm?URI=oe-13-10-3728.
23. A. V. Gorbach and D. V. Skryabin, "Soliton self-frequency shift, non-solitonic radiation and self-induced transparency in air-core fibers," Opt. Express **16**, 4858–4865 (2008) http://www.opticsinfobase.org/abstract.cfm?URI=oe-16-7-4858.
24. W. H. Press, S. A. Teukolsky, W. T. Vetterling, B. P. Flannery, *Numerical recipes: the art of scientific computing*, 3rd ed. (Cambridge University Press, New York, USA, 2007).
25. V. Roppo, M. Centini, C. Sibilia, M. Bertolotti, D. de Ceglia, M. Scalora, N. Akozbek, M. J. Bloemer, J. W. Haus, O. G. Kosareva, and V. P. Kandidov, "Role of phase matching in pulsed second-harmonic generation: Walk-off and phase-locked twin pulses in negative-index media", Phys. Rev. A **76**, 033829 (2007).
26. R. H. Stolen, and J. B. Bjorkholm, "Parametric amplification and frequency conversion in optical fibers", IEEE J. Sel. Top. Quantum Electron. **18**, 1062–1072 (1982).
27. B. C. Stuart, M. D. Feit, S. Herman, A. M. Rubenchik, B. W. Shore, and M. D. Perry, "Nanosecond-to-femtosecond laser-induced breakdown in dielectrics," Phys. Rev. B **53**, 1749–1761 (1996).
28. T. Chaipiboonwong, P. Horak, J. D. Mills, and W. S. Brocklesby, "Numerical study of nonlinear interactions in a multimode waveguide," Opt. Express **15**, 9040–9047 (2007) http://www.opticsinfobase.org/oe/abstract.cfm?URI=oe-15-14-9040.
29. T. Schreiber, T. Andersen, D. Schimpf, J. Limpert, and A. Tünnermann, "Supercontinuum generation by femtosecond single and dual wavelength pumping in photonic crystal fibers with two zero dispersion wavelengths," Opt. Express **13**, 9556–9569 (2005) http://www.opticsinfobase.org/abstract.cfm?URI=oe-13-23-9556.
30. A. Kudlinski and A. Mussot, "Visible cw-pumped supercontinuum," Opt. Lett. **33**, 2407–2409 (2008) http://www.opticsinfobase.org/abstract.cfm?URI=ol-33-20-2407.

1. Introduction

The generation of an ultrawide optical spectrum known as supercontinuum (SC) as a result of cascaded nonlinear optical effects is arguably one of the most spectacular phenomena in nonlinear optics, and nearly 40 years after its discovery by Alfano and Shapiro [1] it is still one of the hottest topics in photonics. SC laser sources generating high brightness, temporally coherent radiation extending from the visible to the near IR with a very low divergence output beam, have become a formidable tool for scientific investigations. Thanks to the advent of microstructured or holey optical fibers (HFs) in the late 1990s and the constant progress in ultrafast laser technology, table-top sources are now available in most optical labs. Exploiting the HF's high nonlinearity and unprecedented group velocity dispersion (GVD) control, SC sources can produce pulses with a broad range of spectral and temporal properties, extending from continuous-wave (CW) to femtosecond pulsed operation and with a central wavelength

#106238 - $15.00 USD Received 12 Jan 2009; revised 11 Feb 2009; accepted 16 Feb 2009; published 1 Apr 2009

ranging from the visible up to the mid-IR [2–4]. Such flexible properties have favored applications in many diverse scientific fields, including optical coherence tomography, metrology, time resolved excitation spectroscopy and optical communications.

Thanks to the combination of nonlinear experiments and numerical simulations based on generalized nonlinear Schrödinger equations (GNLSEs) [5] or nonlinear envelope equations (NEEs) [6, 7], the complex dynamics underlying SC generation in *single mode* fibers are now very well understood. Octave spanning spectra can be obtained by exploiting a combination of nonlinear phenomena which typically include soliton compression and fission, modulation instability, parametric processes, intrapulse Raman scattering, self phase modulation (SPM) and cross phase modulation (XPM) [5]. Single mode guidance in HFs with suitable dispersive properties however requires fibers with a (sub)wavelength-sized core diameter, in which the material damage threshold typically limits the maximum achievable power spectral density to a few mW/nm for ultrashort pulse operation [4] and to more than 50 mW/nm for CW operation [8]. In the ultrashort pulse regime, where the fiber damage rather than the available pump laser power represents the limiting factor, employing fibers with a larger core, operating in a *multimode* regime, represents the obvious solution to increase the achievable power spectral density. Moreover, apart from high-power handling, multimode fibers also have been shown to exhibit a rich variety of novel nonlinear phenomena [9–12], which could be exploited to extend the performances of singlemode fiber-based nonlinear devices.

The theoretical investigation of nonlinear propagation of ultrashort pulses in multimode waveguides however is still a largely unexplored field. The system complexity has restricted the studies presented so far to the two modes of a birefringent fiber [13–16], to the first two spatially distinct modes of an HF [17], or to the four modes of a two-moded birefringent fiber [18, 19]. Recently, we have developed a model for the accurate description of ultrashort pulse propagation in waveguides with an arbitrary number of modes [20]. This model, comprising general third order optical nonlinearities, Raman, self-steepening, polarization, dispersion and intermodal effects, is applied here to study, for the first time, the dynamics of intermodal nonlinear effects contributing to SC generation under femtosecond pulse excitation. Through numerical simulation of a system of coupled GNLSEs, we show that modal symmetries are key to an efficient intermodal power transfer and derive some guidelines for the exploitation of these effects for SC generation at high spectral densities.

The paper is organized as follows. In Sec. 2 we present the multimode model and the simplifications introduced, we discuss its implementation, and present initial results of nonlinear propagation leading to multimode SC generation. We analyze in more detail the intermodal nonlinear effects that lead to power exchange between modes through four-wave mixing (FWM) and produce additional nonlinear phase shift through XPM in Sec. 3 and Sec. 4, respectively. In Sec. 5 we discuss the importance of intermodal walk-off and show an example of how nonlinear effects scale with the fiber size. Finally we conclude our discussion in Sec. 6.

2. Multimode GNLSE and simulation results

The scope of this study is to explore numerically intermodal effects in silica-air HFs which support multiple modes. Since the computational complexity of the multimode GNLSE (MM-GNLSE) scales with the number of modes to the power of M, with $3 < M < 4$ [20], we restrict our analysis to the study of a *moderately* multimode regime. In particular, we focus our attention on a fiber (HF1), which has already been studied experimentally by Cherif et al. [21]. HF1 consists of large circular air holes with pitch $\Lambda = 2.7\ \mu$m and relative hole size $d/\Lambda = 0.93$, which surround a solid core with a diameter of a few optical wavelengths.

Here, we are interested in much shorter propagation distances and higher peak power pumps than employed in [21] to favor intermodal effects, as discussed later in Sec. 5. Moreover, our

#106238 - $15.00 USD Received 12 Jan 2009; revised 11 Feb 2009; accepted 16 Feb 2009; published 1 Apr 2009

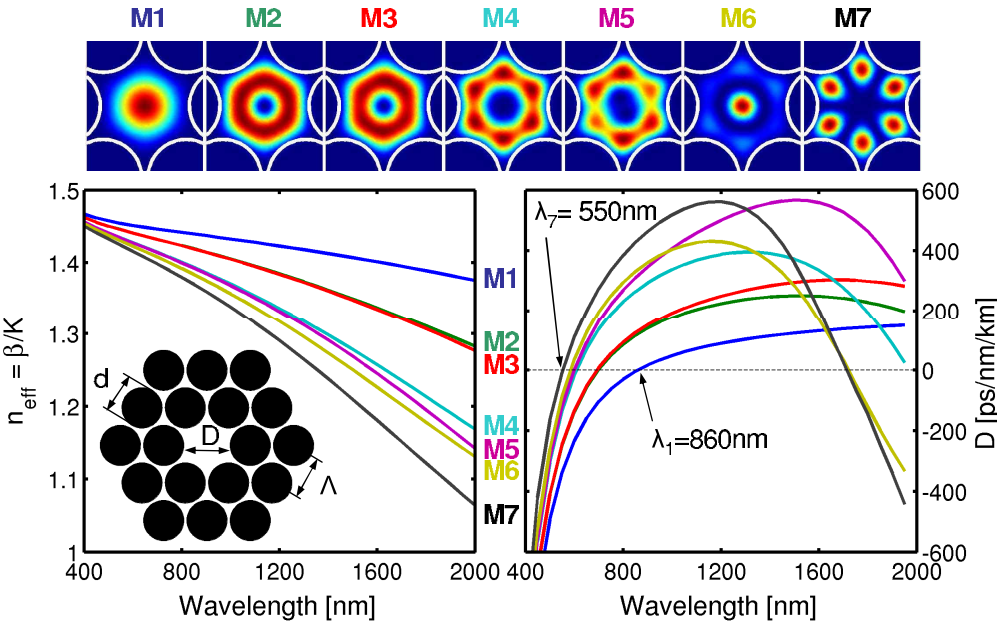

Fig. 1. (Top) Transverse mode functions, calculated at 850 nm, of the 7 circularly polarized modes guided by HF1, an HF with Λ = 2.7 μm and d = 2.5 μm [21]. (Bottom left) Effective index and (bottom right) GVD curves.

model is based on an idealized regular fiber structure which exhibits a slightly larger core, with diameter $D = 2\Lambda - d = 2.9$ μm (see the inset in Fig. 1), for which we do not find any numerical evidence of the high order modes cut off in the near IR discussed in [21]. An accurate full vector finite element method [22] predicts that at least 14 modes with effective areas between 3.6 and 6.1 μm^2 are guided from 400 nm to 2000 nm with low confinement and scattering losses in this fiber. To reduce the computational time required to study nonlinear propagation, we combine them into 7 pairs of circularly polarized modes. Exploiting the forbidden power exchange between modes with opposite circular polarization [20], we only consider the 7 right-handed circularly polarized modes shown in Fig. 1. These are obtained by combining modes HE_{11} (to form mode M1), TE_{01} and TM_{01} (M2), HE_{21} (M3), HE_{31} (M4), EH_{11} (M5), HE_{12} (M6), and EH_{21} (M7). The GVD curves of these modes are remarkably different from each other, with a first zero dispersion wavelength (ZDW) that ranges from $\lambda_7 = 550$ nm for M7 to $\lambda_1 = 860$ nm for M1. M4-M7 also present a second ZDW in the near IR, where they approach their cut-off wavelengths, all positioned beyond 2 μm.

To study the simultaneous nonlinear propagation of multiple modes, we assume that the nonlinear effects do not affect significantly the fiber modes, and hence decompose the electric field of a propagating pulse into a sum of mode functions $\mathbf{F}_n(x,y,\omega)$ with normalization coefficients $N_n(\omega)$, propagation constants $\beta^{(n)}(\omega)$ and longitudinal amplitudes $A_n(z,\omega)$:

$$\mathbf{E}(x,y,z,t) = \sum_n \int \mathrm{d}\omega \, \frac{1}{2} \left\{ \frac{\mathbf{F}_n(x,y,\omega)}{N_n(\omega)} e^{i\beta^{(n)}(\omega)z} A_n(z,\omega) e^{-i\omega t} + c.c. \right\}. \quad (1)$$

#106238 - $15.00 USD Received 12 Jan 2009; revised 11 Feb 2009; accepted 16 Feb 2009; published 1 Apr 2009

The evolution of the amplitude of mode p is then governed by the MM-GNLSE [20]:

$$\frac{\partial A_p(z,t)}{\partial z} = i\left(\beta_0^{(p)} - \beta_0\right)A_p(z,t) - \left(\beta_1^{(p)} - \beta_1\right)\frac{\partial A_p(z,t)}{\partial t} + i\sum_{n\geq 2}\frac{\beta_n^{(p)}}{n!}\left(i\frac{\partial}{\partial t}\right)^n A_p(z,t)$$
$$+ i\frac{n_2\omega_0}{c}\left(1 + i\tau_0\frac{\partial}{\partial t}\right)\sum_{l,m,n}\left\{Q_{plmn}(\omega_0)\Big[2(1-f_R)A_l(z,t)A_m(z,t)A_n^*(z,t)\right.$$
$$\left. + 3f_R A_l(z,t)\int \mathrm{d}\tau\, h(\tau)A_m(z,t-\tau)A_n^*(z,t-\tau)\Big]\right\}, \quad (2)$$

where $f_R = 0.18$ and $h(\tau)$ are the fractional contribution of the Raman response and the delayed Raman response function of silica, respectively. The free parameters ω_0, β_0 and $1/\beta_1$ can be conveniently chosen to represent the central angular frequency of the fundamental mode, its propagation constant and its group velocity, respectively, while $\beta_n^{(p)} = \partial^n\beta^{(p)}/\partial\omega^n|_{\omega=\omega_0}$. The fiber losses are neglected in this study because of the short propagation distances involved. The overlap integrals are rigorously defined as

$$Q_{plmn}(\omega) = \frac{\varepsilon_0^2 n_0^2 c^2}{12}\frac{\int \mathrm{d}x\,\mathrm{d}y\left[\mathbf{F}_p^*(\omega)\cdot\mathbf{F}_l(\omega)\right]\left[\mathbf{F}_m(\omega)\cdot\mathbf{F}_n^*(\omega)\right]}{N_p(\omega)N_l(\omega)N_m(\omega)N_n(\omega)}, \quad (3)$$

where ε_0 and c are the permittivity and the speed of light in vacuum, and n_0 is the silica refractive index at ω_0. Note that Eq. (2) is a simplified version of Eq. (6) in [20], which results from the assumption of the same shock time constant τ_0 for all mode combinations and from the choice of circular polarization, which reduces the number of nonvanishing overlap integrals. Note also that circularly polarized modes were only chosen here because they lead to a significant reduction in computational time; the MM-GNLSE in [20] is otherwise extremely general and allows studying the evolution of pumps with arbitrary polarization states. As most GNLSEs, also the model in (2) assumes that the optical modes are only subject to the nonlinearity of the glass, and that a negligible fraction of power is transmitted in air. This is indeed the case of all the multimode fibers relevant for this study, having a core diameter larger than the pump wavelength, and for which the modal percentage of power in the air holes is always below a few percent (and often below 0.1%).The study of fibers with smaller cores however could be simply tackled by neglecting the air nonlinearity and restricting the integral in (3) only to the glass area. Fibers with multiple glasses or hollow core fibers can still be studied, but they would require modifications to both (3), where $n_0 = n_0(x,y)$ is brought inside the spatial integral, and (2), where the nonlinearity of the second material needs to be included, as in [23].

The system of equations (2) is solved using a standard symmetrized Split-Step Fourier method [13], where adaptive step size control is implemented by propagating the nonlinear operator using a Runge-Kutta-Fehlberg method [24]. In order to avoid numerical artifacts, we also found it necessary to further limit the maximum step size to a fraction of the shortest beat length between all the modes considered. Multiple simulations with increasingly small longitudinal step sizes were run in order to guarantee the accuracy and convergence of the results.

A few simulation results for propagation along 30 mm of HF1 with different launching conditions are shown in Fig. 2. In all cases the pump at launch is centered at $\lambda_p = 850$ nm and has a hyperbolic secant temporal profile $A_p(0,t) = \sqrt{P_0}\,\mathrm{sech}(\mathrm{t}/\mathrm{T}_0)$, with $T_0 = 100$ fs, corresponding to a full width at half maximum $T_{FWHM} = 176$ fs. The pump also initially contains quantum noise. All simulations were performed on a 2^{13} points grid covering the spectral range between 250 nm and 4 μm, and required between 1×10^4 and 2.5×10^4 unequal longitudinal steps.

Figure 2(a) shows the spectral evolution when only M1 is excited at launch and M2-M7 initially contain only quantum noise, a situation that can be approximately achieved by coupling

#106238 - $15.00 USD Received 12 Jan 2009; revised 11 Feb 2009; accepted 16 Feb 2009; published 1 Apr 2009

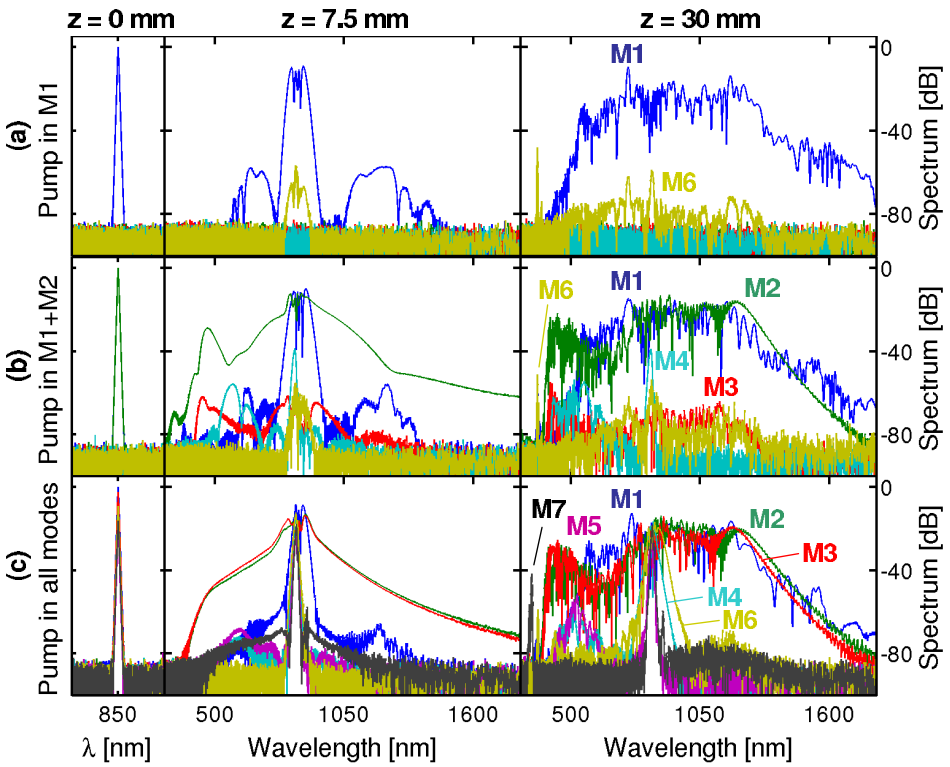

Fig. 2. Examples of multimode nonlinear propagation after 7.5 mm (central column) and 30 mm (right column), for a 100 fs, sech pump centered at 850 nm. (a) Only M1 is excited with a 50 kW peak power pulse; (b) both M1 and M2 are excited with a 50 kW peak power pulse; (c) typical unoptimized launch condition, where a 100 kW Gaussian beam excites M1-M7 with different efficiencies (see main text for details).

an input Gaussian beam with an $1/e$ diameter of 2.4 μm into HF1. The pulse peak power P_0 is set to 50 kW, corresponding to a 10 nJ pulse and, for mode M1, to a soliton of order $N = 166$. As one would expect from single mode SC theory [5], besides SPM-induced spectral broadening, such a high-N pulse develops sidebands which grow spontaneously from noise, through an initial modulation instability (MI) process. The characteristic distance of this phenomenon $L_{MI} \sim 16L_{NL} = \lambda/(6\pi n_2 Q_{1111} P_0) = 6.9$ mm correlates well with the simulation results. More interestingly though, of all the other 6 modes only M6 is significantly amplified at wavelengths around λ_p, and subsequently develops a wide spectral expansion and an isolated peak at 360 nm. Further analysis of the spectrograms and of phase matching conditions [5], seems to suggest that this peak is a dispersive wave, phase matched to a soliton in M1 and slowly shifting to shorter wavelengths as the soliton red-shifts due to the effect of intrapulse Raman nonlinearity. Such an intermodal phase-matching phenomenon certainly deserves additional investigations. Simulations also show that if either M2, M3, M4, M5 or M7 are selectively launched, no power is transferred to any of the other modes, and each of them evolves as in the single mode case.

A very different situation is observed in the Fig. 2(b), representing an idealized situation where both M1 and M2 are simultaneously excited with a $P_0 = 50$ kW sech pulse. This pulse corresponds to an $N = 27$ soliton for M2, due to its much larger value of $\beta_2^{(2)}$ at the pump wavelength. As a result, the SC generated in M2 has a more temporally coherent nature, as it

#106238 - $15.00 USD Received 12 Jan 2009; revised 11 Feb 2009; accepted 16 Feb 2009; published 1 Apr 2009

originates from soliton compression and fission mechanisms (the fission length $L_{fiss} = N \cdot L_{NL}$ is around 16 mm). Due to a shorter ZDW than M1, the final SC in M2 also extends to much shorter wavelengths than the one in M1 (400 nm versus 550 nm, respectively). Moreover, in addition to M6, also M3 and M4 are amplified from noise, generating a complex output spectrum, where the final relative magnitude of different modes is a strong function of wavelength. This is reminiscent of early experimental results [10, 11].

Finally, Fig. 2(c) shows a typical situation of unoptimized coupling. A 100 kW Gaussian input beam with a $1/e$ diameter of 1.2 μm, a horizontal offset of 500 nm and a vertical offset of 100 nm couples into M1-M7 with an efficiency of 42%, 23%, 23%, 3%, 5% and 1% respectively. Due to similar GVD curves, M2 and M3 (which in the weakly guiding approximation form the LP_{11} mode) generate an almost identical, coherent, SC. M4-M7 exhibit some degree of spectral expansion, an evident phase matched dispersive wave peak at 330 nm (M7) and 360 nm (M6), and a pronounced, amplified peak in the visible (M4 and M5). Due to a much longer fission length than M2 however ($L_{fiss} > 40$ mm), all these modes would require an additional propagation distance of 10-15 mm in order to generate an octave spanning SC.

In the following sections we will analyze these results in more detail.

3. Overlap integrals and intermodal power transfer

The results shown in Fig. 2 demonstrate that although much of the fundamental dynamics of singlemode SC generation are maintained for each individual mode of a multimode fiber, additional intermodal effects come into play, stimulating the transfer of power to only selected modes and, as we will discuss later, generating additional nonlinear phase shifts.

Significant insights into the intermodal processes can be gained by analyzing the magnitude and form of the overlap integrals in (3), which control the strength of each nonlinear term. From a quantum mechanical point of view, each Q_{plmn} governs a process extracting one photon each from modes l and m to generate two new photons in modes p and n, respectively, while conserving the total energy. Coefficients of the form Q_{pppp} are therefore responsible for all the intramodal nonlinearities. Coefficients Q_{ppqq} and Q_{pqpq} govern all intermodal XPM effects as discussed in Sec. 4. The remaining overlap integrals control the strength of intermodal FWM effects, which are responsible for all energy transfers between the modes. Figure 3 shows the

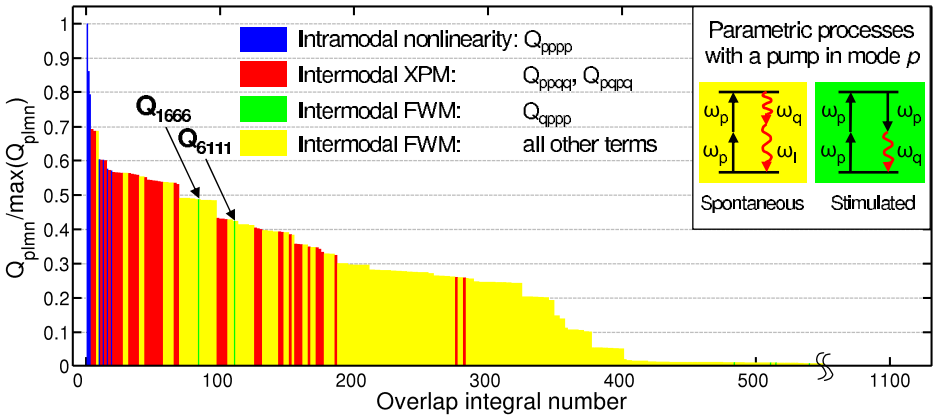

Fig. 3. Normalized overlap integrals for HF1 sorted in descending order. The color codes illustrate the type of nonlinear interaction controlled by each coefficient. The inset shows the two main parametric processes occurring when only the mode p is pumped (see text).

#106238 - $15.00 USD Received 12 Jan 2009; revised 11 Feb 2009; accepted 16 Feb 2009; published 1 Apr 2009

normalized value of all the numerically calculated integrals for HF1. The seven modes give rise to $7^4 = 2401$ terms. More than half of these are identically zero because of symmetry rules [20], and at least 2/3 of the remaining nonzero terms are small enough to be neglected without appreciable differences in the results.

If only a single mode p is pumped with a narrow spectral line, intermodal power transfer is mediated by degenerate FWM terms of the form Q_{qppl}. If both modes q and l are initially empty, power transfer starts with a spontaneous FWM process and is therefore slow. On the other hand, processes where one of the generated photons is returned into the pump p by *stimulated emission* (Fig. 3, inset) are much faster and are therefore the dominant FWM processes in the limit of high-power pulse propagation over short distances. Interestingly, these processes Q_{qppp} produce the automatic phase-locking of mode q to the pump mode, similarly to to what happens in non-phase matched second and third harmonic generation processes [25]. However, processes Q_{qppp} require that (i) modes p and q belong to the same symmetry class, and (ii) that they present a large overlap. For HF1 these conditions are only fulfilled for the two LP_{0n} modes M1 and M6, as shown in Fig. 3, and this explains the results in Fig. 2(a) where nonlinear coupling is only observed between these two modes.

When two or more modes contain a significant amount of power, they can all act as pumps for weaker modes. Moreover, if these modes belong to different symmetry classes, additional FWM terms come into play giving rise to the rich phenomenology seen in Fig. 2(b). Figure 4 shows the initial evolution of this pulse propagation, where a spectral offset was imposed on the two pumps and intramodal nonlinear effects were neglected for clarity. Figure 4(a) shows that after a propagation of 0.4 mm, well defined spectral peaks develop from the initial noise in all the 5 remaining modes at frequencies that satisfy energy conservation. Some of the overlap integrals responsible for these intermodal FWM processes are indicated in the figure. Note that modes M5 and M7 are pumped through cascaded FWM processes, where in an intermediate step power is first transferred from M1 and M2 to M3 and M4 and only later to M5 and M7.

The evolution of the gain experienced by each mode in the simulation is shown in Fig. 4(b).

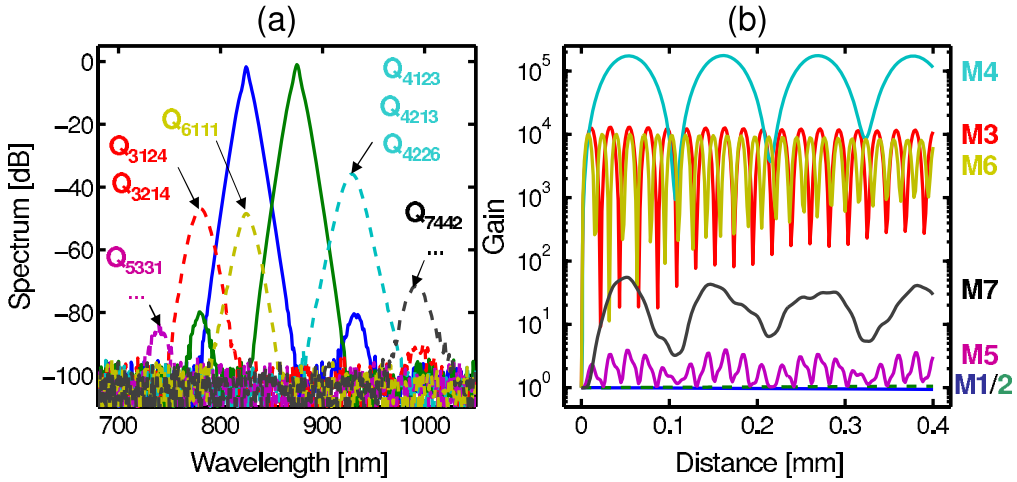

Fig. 4. (a) Multimode output spectrum after 0.4 mm propagation in HF1, where two signals where launched in M1 and M2 with a spectral offset and $P_0 = 100$ kW (solid lines). Dashed lines indicate signals amplified from noise through intermodal FWM. The color code is shown on the extreme right. (b) Dynamic gain evolution for each individual mode showing the oscillatory behavior typical of non phase-matched parametric processes.

#106238 - $15.00 USD Received 12 Jan 2009; revised 11 Feb 2009; accepted 16 Feb 2009; published 1 Apr 2009

The observed oscillatory behavior can be explained by the simple approximate analytic theory for CW pumped parametric processes, which neglects the effects of GVD and pulse walk-off [26]. Within this framework, parametric gain leading to exponential signal amplification happens if the propagation constant mismatch $\Delta\beta_{plmn} = \beta^{(l)}(\omega_l) + \beta^{(m)}(\omega_m) - \beta^{(p)}(\omega_p) - \beta^{(n)}(\omega_n)$ is smaller than a few times the average inverse nonlinear length $1/L_{NL} = \overline{\gamma}P_0$. For multimode processes, an estimate of $\overline{\gamma}$ can be obtained by averaging all the intermodal nonlinearities $\gamma_{plmn} = \frac{6\pi n_2}{\lambda} Q_{plmn}$ which contribute to SPM and XPM between the relevant modes. However, for the tightly confined modes in HF1 we find $\Delta\beta_{plmn} \gg \overline{\gamma}P_0$ for all the relevant FWM processes considered. Thus, no parametric gain is observed, and each FWM term leads to the oscillatory power exchange between modes shown in Fig. 4(b), with oscillation periods given by the beat lengths $L_b \sim 2\pi/|\Delta\beta|$. For example, for the process leading to amplification of M6, $\Delta\beta_{6111} = 4.1 \cdot 10^5$ m^{-1}, corresponding to a value of $L_b = 15.3$ μm in agreement with the simulation. Note that even for P_0 equal to the damage threshold for this fiber (estimated as 900 kW for 100 fs pulses [27]), we obtain $\overline{\gamma}P_0 = 4.7 \cdot 10^4$ m$^{-1} \ll \Delta\beta_{6111}$. Therefore the conditions for exponential signal growth can never be satisfied for this fiber, although they may be reachable in small index contrast, conventional fibers, where $\Delta\beta$ is much smaller. Modes M5 and M7 are pumped by cascaded processes, as discussed above, and therefore do not exhibit amplitude fluctuations governed by a single beat length. Finally, M1 and M2 are not significantly depleted under these operating conditions, despite transferring power to all the other modes, and thus appear as constant in Fig. 4(b).

Despite the initial power oscillation between modes, all the simulations preformed indicate that after a long enough propagation some power is *permanently* transferred into the weaker modes, even if no effort is made to phase match the process. This is shown for M4 in Fig. 5 extending the propagation of Fig. 4(b) from 0.4 mm to 4 mm. A more detailed analysis excluding XPM and Raman effects found this behavior to be uniquely caused by the temporal *walk-off* between the pulses involved. The typical length scale of this permanent power transfer is therefore of the order of the walk-off length of all the pulses involved, given by $L_W^{pq} = T_0/|1/v_g^{(p)} - 1/v_g^{(q)}| = T_0/|\beta_1^{(p)} - \beta_1^{(q)}|$ for modes p and q. For the example in Fig. 5, $L_W^{12} = 3$ mm, $L_W^{24} = 2.4$ mm and $L_W^{14} = 1.3$ mm, which correlate well with the simulation.

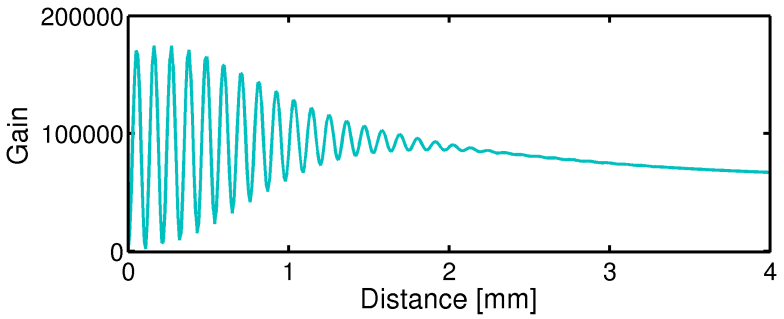

Fig. 5. Longitudinal evolution of the gain of M4 under the same conditions as in Fig. 4.

4. Intermodal cross phase modulation

Having discussed the effect of the intermodal FWM terms, which can transfer power between modes even in the absence of proper phase matching, it is now instructive to study the effect of intermodal XPM. To do so, we simulate the propagation of a pulse launched in M1 and/or M2 at 725 nm, where M1 is in the normal dispersion regime and M2 is in the anomalous regime. In

#106238 - $15.00 USD Received 12 Jan 2009; revised 11 Feb 2009; accepted 16 Feb 2009; published 1 Apr 2009

order to observe significant spectral expansion and intermodal effects within the distance where the pulses are temporally overlapped, we increased the input power up to a value of $P_0 = 500$ kW, close to the estimated fiber damage threshold.

Figures 6(a) and (b) show that when M1 is individually launched, only some SPM-based spectral expansion is visible, whereas if only M2 is launched, a wide MI-based SC develops. On the other hand, if the same input pulse is launched *simultaneously* in both modes as in Fig. 6(c), a much wider output spectrum is produced in M1. Under these conditions there is negligible power transfer between the two modes, which is confirmed by nearly identical spectral results obtained with additional simulations when all Q_{plmn} coefficients responsible for intermodal FWM are set to zero. Figure 6(d) however shows that if all intermodal XPM effects are switched off, M1 and M2 produce a spectrum very similar to that of their individual propagation. This demonstrates that intermodal XPM effects can generate significant nonlinear phase shifts leading to extended spectral broadening [28, 29].

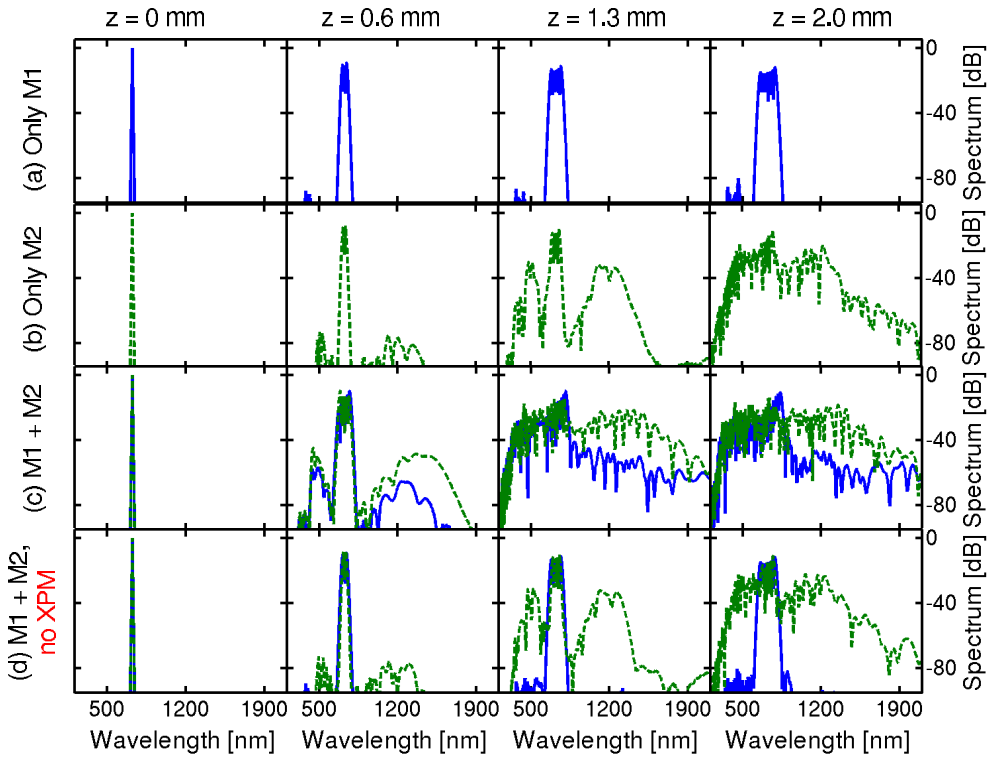

Fig. 6. Propagation of a $T_0 = 100$ fs and $P_0 = 500$ kW sech pulse centered at 725 nm and launched in: (a) M1 only (blue, solid line); (b) M2 only (green, dashed line); (c) both M1 and M2, and (d) both M1 and M2 when all intermodal XPM coefficients are set to zero.

5. Fiber diameter and high power scaling

In Sec. 3 we have seen that intermodal power transfer is governed by two different length scales: (i) the beat length L_b is related to the phase velocity mismatch and determines the period of the fast power oscillations at the onset of the nonlinear dynamics; (ii) the walk-off length L_W is related to the group velocities and determines the distance over which power is permanently transferred. A necessary condition for efficient permanent multimode power transfer therefore

#106238 - $15.00 USD Received 12 Jan 2009; revised 11 Feb 2009; accepted 16 Feb 2009; published 1 Apr 2009

is that nonlinear processes occur within L_W, that is, the nonlinear length L_{NL} must fulfill

$$L_{NL} < L_W, \tag{4}$$

where L_{NL} and L_W are assumed to be averaged over all the processes one is interested to maximize. For a given multimode fiber and a specific wavelength of operation, L_W depends linearly only on the pulse duration T_0, while L_{NL} is inversely proportional to the peak power P_0. Therefore, P_0 and T_0 can in principle be independently tuned.

Operating significantly outside the range given by (4) ensures that multimode intermodal effects can safely be neglected. This is useful for applications where nonlinear effects are detrimental and explains why in many experimental studies employing moderately multimode fibers intermodal nonlinear effects are often not observed [4, 21]. In this paper, however, we are concerned with the opposite limit of significant intermodal nonlinear effects, and therefore focus on the parameter regime prescribed by (4).

Transmission of femtosecond pulses in a few-moded fiber such as HF1 typically produces L_W of only a few mm. Eq. (4) thus implies operating at high peak powers such as those chosen for the simulations in Fig. 2. This choice also has implications for the *coherence* properties of the overall multimode SC. Although this is certainly a complex issue, which deserves further dedicated studies, we can still make a few general comments. Launching such a pump close to a mode ZDW typically produces a soliton number $N \gg 40$ and hence leads to the generation of a MI-based, incoherent SC [2, 5]. In other modes, further away from a ZDW, the same pump may correspond to values of N of 15-40 or lower, required to produce a soliton-fission based SC with a high degree of coherence. The two types of SC can exist simultaneously in a multimode fiber as clearly shown in Fig. 2(b) and (c). If intermodal FWM effects take place, the coherence of the pump signal(s) is generally not transferred to the signal and idler pulses. An exception to this takes place in those processes governed by terms of the form Q_{qppp} where, as previously observed [25], the phase of mode q is automatically locked to that of mode p. We expect therefore that in this case the overall pump coherence will be transferred to mode q, even if this is initially amplified from noise.

Having analyzed in detail the multimode nonlinear dynamics for a specific fiber, it is now interesting to study how the nonlinear effects scale with the fiber dimensions. Figure 7 shows the simulated optical properties of three fibers with the same structure as HF1, i.e., the same value of d/Λ, but a core diameter either smaller than HF1 (HF2, $D = 1\ \mu$m), similar to HF1 (HF3, $D = 3\ \mu$m), or significantly larger than HF1 (HF4, $D = 10\ \mu$m). Only the first 16 linearly polarized modes are shown. As the number of guided modes scales with D^2, these fibers present noticeably different behaviors, ranging from single mode guidance at $\lambda > 1300$ nm for HF2, to the guidance of more than 80 modes at 1550 nm in HF4.

In the *small core* regime ($D \lesssim \lambda_p$), fiber HF2, all modes present two zero dispersion wavelengths, but the spectral regions of anomalous dispersion differ widely. In this case it is possible to tailor the position of phase and/or group velocity matched wavelengths between selected modes for the generation of optimized nonlinear devices based on intermodal nonlinear effects. However, glass damage limits the maximum pulse energy that can be transmitted in these fibers. *Large core* fibers with $D \gg \lambda_p$, such as HF4 in Fig. 7, present the simplest solution to scale up the damage threshold. On the other hand, in this case the GVD of all modes tends to that of the core material. This restricts the flexibility to selectively enhance or suppress specific intermodal nonlinear processes by dispersion control. In the *intermediate* regime, fibers HF1 and HF3, some features of both the small core and the large core limit persist, leading to the broad range of nonlinear effects seen in Fig. 2.

The bottom row of Fig. 7 displays the group delay difference gdd = $(1/v_g^{(1)} - 1/v_g^{(2)}) = T_0/L_W^{12}$ for fibers HF2-HF4. For example, the gdd between the LP_{01} and LP_{02} modes at 850

#106238 - $15.00 USD Received 12 Jan 2009; revised 11 Feb 2009; accepted 16 Feb 2009; published 1 Apr 2009

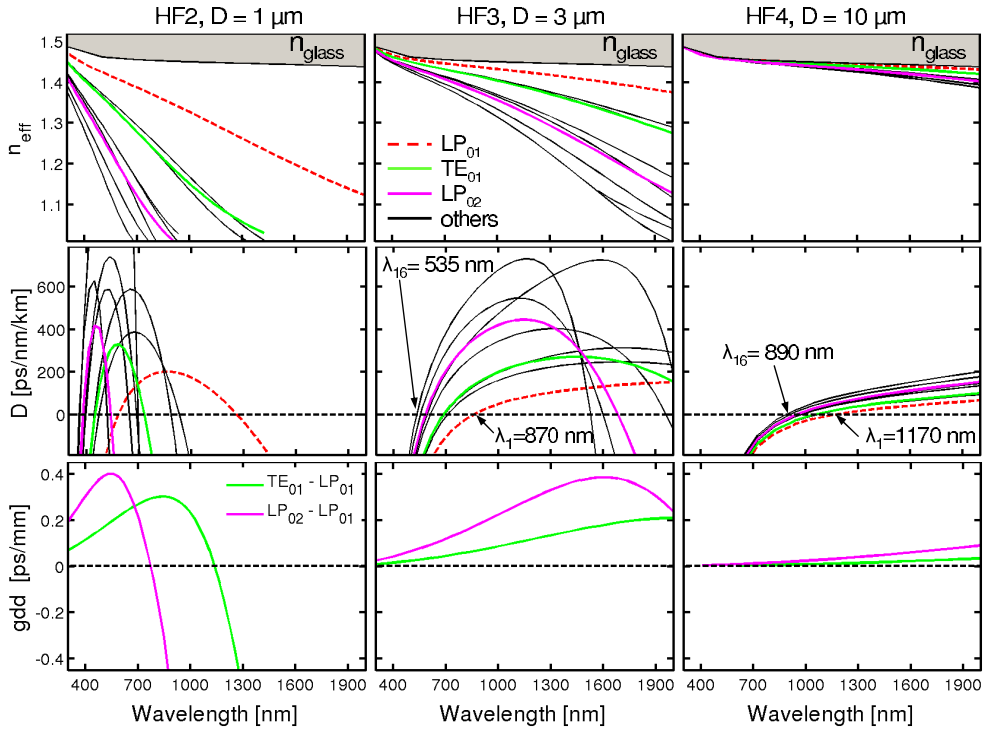

Fig. 7. Optical properties of three HFs with the structure shown in the inset of Fig. 1 and different core diameters D. Only the first 16 modes are shown. The top row shows the effective index (n_{eff}) of the modes; the middle row shows the dispersion curves; the bottom row shows the group delay difference (gdd) between two pairs of modes. Red, green and pink lines indicate the HE_{11} (M1), TE_{01} (M2) and HE_{12} (M6) modes, respectively.

nm is -0.31 ps/nm for HF2, 0.16 ps/nm for HF3 and 0.017 ps/nm for HF4. This leads to a much longer walk-off length in HF4 and thus, according to (4), noticeable intermodal nonlinear effects can be observed in HF4 even at relatively low peak powers.

The power scaling of multimode SC generation with core size D is investigated in Fig. 8 where we show the simulated output energy spectral density (ESD) for HF1 ($D = 2.9\ \mu$m) and HF4 ($D = 10\ \mu$m) for a pump exclusively in the LP_{01} mode. Generalizing our earlier result from Sec. 3 that in this case intermodal FWM is dominated by Q_{qppp} terms, we restricted the simulations to the LP_{0n} modes, with $n = 1,2$ for HF1 and $n = 1...6$ for HF4. To obtain a fair comparison between two fibers with such different dispersive and nonlinear properties, we chose launch conditions giving the same fluence and input soliton number (i.e., similar L_{NL}), and studied the pulse evolution over the same distance of 30 mm. For HF1 we used the same pump parameters as in Fig. 2(a), i.e., $P_0 = 50$ kW and $\lambda_p = 850$ nm, while for HF4, as a result of the ~ 15 times larger effective area, we used a sech pulse with $P_0 = 753$ kW, launched at $\lambda_p = 1185$ nm. Note that, for numerical reasons, these input energies are still ~ 10 times below the damage threshold and that an order of magnitude higher ESD could therefore be achieved in practice.

Figure 8 shows that under these conditions both fibers develop a spectrally flat SC in LP_{01} spanning more than one octave, but the higher input power used for HF4 produces a SC with a correspondingly higher ESD. A striking difference is however evident for the higher order modes. Whereas the output from HF1, apart from the dispersive wave peak in the UV, can

#106238 - $15.00 USD Received 12 Jan 2009; revised 11 Feb 2009; accepted 16 Feb 2009; published 1 Apr 2009

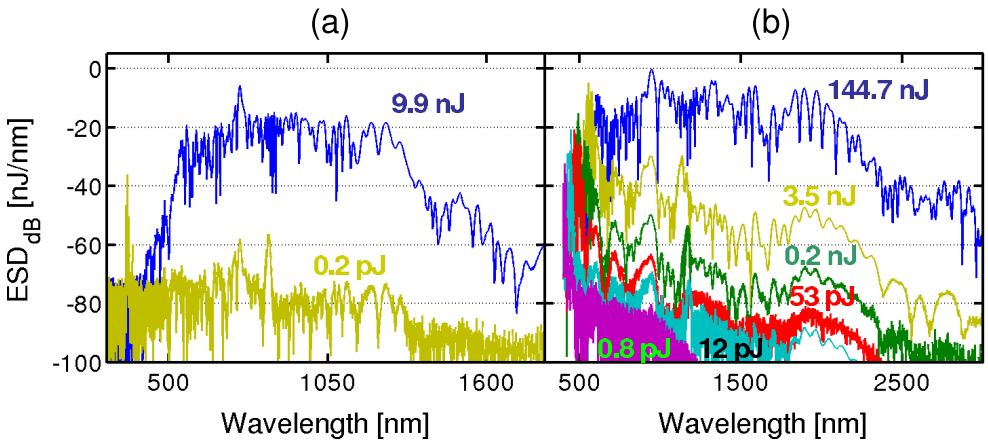

Fig. 8. Output energy spectral density (ESD) after propagation in 30 mm of (a) HF1 and (b) HF4, when only the LP_{01} mode (blue) is launched. Only the LP_{0n} higher order modes are considered: LP_{02} (yellow), LP_{03} (green), LP_{04} (red), LP_{05} (cyan), LP_{06} (magenta). The total output energy in each mode is indicated next to each curve. Input conditions for HF1 are the same as in Fig. 2(a); the same input fluence and soliton number N were used for the pump in HF4, by launching it with $P_0 = 753$ kW and at $\lambda_p = 1185$ nm.

be considered as single mode, the overall output beam from HF4 contains $> 2.5\%$ of energy in the higher order modes. Thus, a 15-fold increase in input power between Figs. 8(a) and (b) increases the power transferred to LP_{02} by four orders of magnitude as a result of the longer beat length L_b and walk-off length L_W for the large-core fiber HF4. There is also a vast difference of power transfer efficiency between the fundamental and the various higher order modes of HF4, which we attribute to the increasing phase mismatch, from $\Delta\beta = 5.16 \times 10^4$ m^{-1} for LP_{02} to 4.89×10^5 m^{-1} for LP_{06}, and the decreasing coupling strength, from $\gamma_{2111} = 1.52$ W^{-1}km^{-1} to $\gamma_{6111} = 0.03$ W^{-1}km^{-1}.

Finally, we also note in Fig. 8(b) that although the total energy transferred to the higher order modes is more than 40 times lower than the energy in the fundamental mode, all LP_{0n} modes form a dispersive wave peak in the visible, phase matched to a soliton in the fundamental mode, and carrying more energy than the LP_{01} mode at the same wavelengths. Therefore, as already suggested [19,30], large-core fibers allow for extended SC spectra towards shorter wavelengths, albeit at the cost of reduced spatial homogeneity because of the multimode structure of the output.

6. Summary and conclusion

Through numerical simulations we have analyzed the nonlinear dynamics of ultrashort pulses propagating in moderately multimode fibers. Cross phase modulation was found to be able to significantly broaden the spectral output of modes which do not exhibit supercontinuum generation if pumped on their own. Intermodal four-wave mixing can result in significant transfer of power from pumped modes into higher order modes.

We have identified the main nonlinear processes responsible for multimode supercontinuum generation. Simultaneously pumping several modes of different symmetries leads to power transfer into all higher order modes regardless of their symmetry by direct or cascaded four-wave mixing processes. If only the fundamental LP_{01} mode is pumped, the dominant nonlinear mechanisms only couple light into other LP_{0n} modes via stimulated processes which involve

#106238 - $15.00 USD Received 12 Jan 2009; revised 11 Feb 2009; accepted 16 Feb 2009; published 1 Apr 2009

three pump photons, and phase-lock the generated modes to the pump. In this case the number of modes included in the numerical analysis can be significantly reduced and high-power pulse propagation in heavily multimoded fibers may become tractable numerically.

Nonlinear intermodal power transfer is governed by two length scales, a beat length leading to fast initial power oscillations and a walk-off length leading to permanent power transfer. In order to observe these nonlinear effects, the nonlinear length of the pump pulses must be shorter than the walk-off length, i.e., high peak powers are required. Otherwise, nominally multimode fibers can behave, nonlinearly, as single mode ones. Scaling a fixed fiber structure to larger core sizes allows for larger power throughput, but at the same time longer beat and walk-off lengths lead to much stronger mode coupling, and significant amounts of power are transferred to higher order modes. In this case, higher order modes may also serve to extend the overall supercontinuum to much shorter wavelengths.

We believe that such a detailed study of intermodal nonlinear dynamics will provide useful guidelines for the generation of SC with record-high power spectral density and for the fabrication of nonlinear multimode devices with improved performances. This paper provides only a preliminary investigation into the vast research area of multimode nonlinear effects, which has the potential to become an increasingly important theme for any extremely high power laser transmission. Further studies into phenomena only briefly mentioned in this work, such as the intermodal FWM-mediated phase locking effect or the intermodal phase matching between solitons and dispersive waves, as well as experimental verifications of the main results and scaling rules discussed here seem the next logical step.

Acknowledgments

This work was supported by the UK Engineering and Physical Sciences Research Council (EPSRC) through Grant EP/E056369/1.

#106238 - $15.00 USD Received 12 Jan 2009; revised 11 Feb 2009; accepted 16 Feb 2009; published 1 Apr 2009